Hot tropical temperatures during the Paleocene-Eocene thermal maximum revealed by paired in-situ $\delta^{13}C$ and Mg/Ca measurements on individual planktic foraminifer shells

Reinhard Kozdon [1], D. Clay Kelly [2]

[1] Lamont-Doherty Earth Observatory of Columbia University, Palisades, New York 10964, USA; [2] Department of Geoscience, University of Wisconsin, Madison, Wisconsin 53706, USA

Corresponding author: Reinhard Kozdon (rkozdon@ldeo.columbia.edu)

Key points:

- Microanalytical techniques used to measure paired $\delta^{13}C$ and Mg/Ca ratios in individual foraminifer shells from a pelagic PETM record
- $\delta^{13}C$ values of individual foraminifers used to identify and exclude reworked non-PETM specimens from Mg/Ca-based SST record
- Unmixed Mg/Ca-based temperature record indicates tropical SSTs increased by ~6ºC in central Pacific Ocean during PETM

Abstract

The Paleocene-Eocene thermal maximum (PETM, 56 Ma) is an ancient global warming event closely coupled to the release of massive amounts of ^{13}C-depleted carbon into the ocean-atmosphere system, making it an informative analogue for future climate change. However, uncertainty still exists regarding tropical sea-surface temperatures (SSTs) in open ocean settings during the PETM. Here, we present the first paired δ^{13}C:Mg/Ca record derived in-situ from relatively well-preserved subdomains inside individual planktic foraminifer shells taken from a PETM record recovered in the central Pacific Ocean at ODP Site 865. The δ^{13}C signature of each individual shell was used to confirm calcification during the PETM, thereby reducing the unwanted effects of sediment mixing that secondarily smooth paleoclimate signals constructed with fossil planktic foraminifer shells. This method of 'isotopic screening' reveals that shells calcified during the PETM have elevated Mg/Ca ratios reflecting exceptionally warm tropical SSTs (~33-34ºC). The increase in Mg/Ca ratios suggests ~6°C of warming, which is more congruent with SST estimates derived from organic biomarkers in PETM records at other tropical sites. These extremely warm SSTs exceed the maximum temperature tolerances of modern planktic foraminifers. Important corollaries to the findings of this study are (1) the global signature of PETM warmth was uniformly distributed across different latitudes, (2) our Mg/Ca-based SST record may not capture peak PETM warming at tropical Site 865 due to the thermally-induced ecological exclusion of planktic foraminifers, and (3) the record of such transitory ecological exclusion has been obfuscated by post-depositional sediment mixing at Site 865.

Plain Language Summary

The Paleocene-Eocene thermal maximum (PETM, about 56 million years ago) is a global warming event that is widely regarded as an ancient analogue for climate change being driven by the current rise in atmospheric carbon dioxide (CO_2) levels. Accurate measurements of PETM warmth in the tropical oceans are crucial to validating climate model simulations and gauging the effect of global warming on oceanic ecosystems. However, chemical analyses of marine microfossils (foraminifera) typically yield tropical sea surface temperatures (SSTs) for the PETM that are cooler than those computed by climate models. Primary reasons for this discrepancy are poor preservation of the foraminifer shells and displacement of shells from the cooler pre-PETM interval into overlying PETM sediments via sediment mixing processes. Here, we use in-situ microanalytical techniques to measure both the carbon isotope composition (δ^{13}C) and Mg/Ca ratio within the same individual shells. The δ^{13}C values of shells were used to identify displaced pre-PETM specimens with higher, background δ^{13}C ratios and exclude them from our Mg/Ca-based temperature record. Our new "isotopically filtered" Mg/Ca-based temperature record suggests ~6°C of warming in the

tropical Pacific, with SSTs (33-34°C) likely exceeding the maximum temperature tolerances of many calcifying plankton during the PETM.

1. Introduction

The Paleocene-Eocene thermal maximum (PETM, circa 56 Ma) is one of the most dramatic global warming events in Earth's history. Geochemical records show that sea surface temperatures (SSTs) warmed globally by ~4 to 6°C (Dunkley Jones et al., 2013; Inglis et al., 2020; Tierney et al., 2022) and that this transient (~170 ka) warming was coupled to a major perturbation of Earth's surficial carbon cycle with a sustained period of ocean acidification (Gutjahr et al., 2017; Penman et al., 2014; Zachos et al., 2005; Zeebe and Lourens, 2019). In geological records, a global hallmark of the PETM is a negative carbon isotope excursion (CIE) signaling the release of massive quantities of previously sequestered, ^{13}C-depleted carbon into the ocean-atmosphere system (Dickens et al., 1995; Kennett and Stott, 1991; Kirtland Turner et al., 2017; Koch et al., 1992). First recognized over thirty years ago (Thomas, 1989), the PETM is now considered a natural analogue for climate change being driven by the current rise in atmospheric carbon dioxide (CO_2) levels and thus provides a test case for assessing the accuracy of climate models simulating the response of the Earth system to rapid greenhouse-gas driven warming.

However, despite considerable effort, model-data mismatches still exist as well as inconsistencies between PETM reconstructions based on different proxies (e.g., Hollis et al., 2019; Lunt et al., 2013). Particularly challenging is the tendency for proxy-based tropical SSTs to be cooler than SSTs calculated by PETM model simulations. Proxy-based paleoclimate reconstructions suggest that the mid- to high-latitude surface oceans approached, or even exceeded, modern tropical temperatures (24°C to 29°C) during the PETM (e.g., Sluijs et al., 2011; Zachos et al., 2006). Climate model simulations indicate that this degree of mid-latitude warming should be accompanied by tropical SSTs ≥35ºC (Huber, 2008; Lunt et al., 2012). To date, such extremely warm tropical temperatures for the PETM have been recorded by only a handful of proxy-based SST records from coastal and hemi-pelagic settings (e.g., Aze et al., 2014; Frieling et al., 2017). A dearth of robust proxy-based tropical SST reconstructions for PETM records from pelagic settings has exacerbated this problem.

The paucity of robust tropical SST reconstructions for the PETM from pelagic settings is chiefly due to vagaries of the fossil record. Diagenetic recrystallization has been particularly troublesome for SST reconstructions based on the oxygen isotope (δ^{18}O) compositions of planktic foraminifer calcite. The recrystallization of foraminifer shells typically takes place on the seafloor or within the upper sediment column at temperatures that are colder than the overlying tropical surface waters where the shells originally calcified (e.g., Pearson et al., 2001; Schrag et al., 1995; Sexton et al., 2006). Aside from imparting a 'frosty' hue to foraminifer shells, recrystallization can be difficult to detect because it usually occurs on micrometer scales (Pearson et al., 2001; Wilson et al., 2002). Thus, conventional isotope ratio mass spectrometers requiring analysis of whole shells may include diagenetic calcite, which artificially elevates the measured $\delta^{18}O$ compositions and biases tropical SST estimates towards cooler (bottom water) temperatures.

Tropical SST reconstructions for the PETM can also be biased towards lower temperatures by sediment mixing. In most pelagic settings, the uppermost ~8 cm of the sediment column is thoroughly mixed by the burrowing activities of benthic organisms (bioturbation) prior to being incorporated into the deep-sea sedimentary record (Berger and Johnson, 1978; Berger and Heath, 1968). The time-averaging effects of this sediment mixing typically smooths paleoclimate records over millennial time scales (e.g., Hull et al., 2011; Hutson, 1980; Peng et al., 1979), which can be problematic for reconstructions of abrupt, transitory paleoclimate events. Astronomical tuning of deep-sea sedimentary records constrains the duration of the PETM to ~170,000 years (Röhl et al., 2007; Zeebe and Lourens, 2019) and computational models indicate that the onset of PETM conditions took <5 kyr (Kirtland Turner et al., 2017; Zeebe et al., 2016). Hence, pelagic PETM records deposited at relatively slow sedimentation rates are highly susceptible to blending by sediment mixing, especially across their basal parts where the stratigraphic record has been condensed by CO_2-induced carbonate dissolution (Kirtland Turner et al., 2017; Thomas et al., 2002; Zachos et al., 2005).

The degree to which pelagic PETM stratigraphies are distorted by sediment mixing was more fully appreciated by studies that used the $\delta^{13}C$ compositions of individual planktic foraminifers to distinguish CIE specimens with relatively low $\delta^{13}C$ values from non-CIE specimens with higher $\delta^{13}C$ values that had been displaced (reworked) into the CIE interval (Kelly et al., 1996; Thomas et al., 2002; Zachos et al., 2007). This method of geochemically screening planktic foraminifer shells is predicated on the premise that the rapid decrease in ocean-atmosphere $\delta^{13}C$ composition imparted a distinctive $\delta^{13}C$ signature to only those shells grown during the PETM; hence, CIE shells register $\delta^{13}C$ values that are approximately 4-5‰ lower than those recorded by non-CIE shells (Hupp et al., 2023; Kozdon et al., 2018). In short, the $\delta^{13}C$ signature of the CIE can be used as a 'time-marker', making it possible to identify shells calcified during the PETM and exclude reworked non-CIE shells that would otherwise bias tropical PETM SST records towards cooler pre-PETM temperatures.

In this study, we revisit the well-studied PETM record from Ocean Drilling Program (ODP) Site 865 to reconstruct tropical SSTs in the central Pacific Ocean. We mitigate the detrimental effects of diagenesis and sediment mixing by using in-situ microanalytical techniques to make "paired" $\delta^{13}C$ and magnesium:calcium (Mg/Ca) ratio measurements on micrometer-scale subdomains within individual planktic foraminifer shells. The microanalytical techniques herein employed are relatively non-destructive and conserve the bulk of the shell, making it possible to measure $\delta^{13}C$ and Mg/Ca ratios in tandem within the same individual shell. As described above, the $\delta^{13}C$ values are used to identify and exclude reworked non-CIE specimens from our Mg/Ca-based SST reconstruction for the PETM. The Mg/Ca ratio of a planktic foraminifer shell is primarily controlled by calcification temperature and thus allows for the reconstruction of past SSTs (e.g., Lea et al., 1999). An added advantage of using foraminifer Mg/Ca ratios is that it circumvents uncertainties regarding short-term changes in local seawater $\delta^{18}O$ composition that influence the $\delta^{18}O$ composition of planktic foraminifer shells. This particular aspect of Mg/Ca paleothermometry is deemed advantageous as spatial patterns in seawater $\delta^{18}O$ variability were altered during the PETM (Kozdon et al., 2020; Pagani et al., 2006; Rush et al., 2021; Zachos et al., 2003). Moreover, studies (Sexton et al., 2006; Staudigel et al., 2022) have shown that the Mg/Ca proxy is less sensitive to diagenetic alteration than the $\delta^{18}O$ proxy in planktic foraminifer shells. Thus, Mg/Ca ratios can yield more reliable SSTs from partially recrystallized shells with compromised $\delta^{18}O$ values.

2. Material and Methods

2.1. Study Site and Core Sampling

The Site 865 PETM record was recovered from atop Allison Guyot (18°26.425'N, 179°33.339'W) at a water depth of 1517.4 meters in the Mid-Pacific Mountains (Fig. 1) (Sager et al., 1993). Benthic foraminifer assemblages indicate that this PETM record was deposited at mid-bathyal (~1,300 m) water depths and paleolatitude projections place Site 865 near the equator (~2-5º N) during the Paleocene (Bralower and Mutterlose, 1995; Sager et al., 1993). Sample selection was guided by previously published $\delta^{13}C$ records (Bralower et al., 1995; Hupp et al., 2022) and biostratigraphic studies (Kelly et al., 1996), which constrained the PETM record to a thin (~16 cm) stratigraphic interval positioned between 103.00 and 102.84 meters below sea floor (mbsf) in Core 12H from hole 865C. The study section (105.00 – 100.50 mbsf) is composed of weakly lithified, calcareous ooze and was sampled at varying resolutions, 3-10 cm within the CIE interval and 2-110 cm outside the CIE interval (Fig. 1). The age model previously constructed by Kozdon et al. (2011) for the Site 865 PETM record is used in this study (Table 1). Foraminifer shells were gleaned from the bulk-sediment samples by rinsing the sediment with pH buffered (~8.0), deionized water over a 63-µm sieve. All planktic foraminifer shells have been partially recrystallized via carbonate diagenesis, as indicated by their opaque, stark white appearance under reflected light (e.g., Pearson et al., 2001; Wilson et al., 2002) and the secondary thickening of muricae protuberances into blade-like structures along the exteriors of the shell walls (Sexton et al., 2006).

Planktic foraminifer shells were handpicked under a stereo light microscope from the processed residues of each sample taken from Site 865 PETM section. The planktic foraminifer species *Morozovella velascoensis* and *M. allisonensis* were targeted for SST reconstruction. Both taxa are fairly common within the CIE interval at Site 865, with *M. velascoensis* occurring throughout the entire 4.5-meter study section whilst the 'excursion taxon', *M. allisonensis*, occurs only within the CIE interval (Kelly et al., 1996). The limited stratigraphic range of the short-lived *M. allisonensis* makes it a reliable marker for the PETM (Pearson et al., 2006). The stable isotope ($\delta^{18}O$, $\delta^{13}C$) signatures of these two taxa indicate calcification within the oceanic mixed layer of the surface ocean, making them prime candidates for SST reconstructions (D'Hondt et al., 1994; Kozdon et al., 2011; Kozdon et al., 2013; Norris, 1996; Shackleton et al., 1985). Initially, *M. allisonensis* was thought to have calcified in cooler, deeper waters owing to its relatively heavier $\delta^{18}O$ signature (Kelly et al., 1996; Kelly et al., 1998), but subsequent study has shown that the higher $\delta^{18}O$ values are an artifact of carbonate diagenesis and that *M. allisonensis* was actually a surface-ocean dweller (Kozdon et al., 2011). The $\delta^{13}C$ signatures of *M. velascoensis* and *M. allisonensis* covary positively with increasing shell size (D'Hondt et al., 1994; Kelly et al., 1998; 2001). Similar $\delta^{13}C$/size trends occur among modern planktic foraminifers that host algal photosymbionts and calcify their shells within the euphotic zone of the oceanic mixed layer (D'Hondt et al., 1994; Norris, 1996), thus *M. velascoensis* and *M. allisonensis* are considered to have had a similar photosymbiotic ecology. As a result, our paired $\delta^{13}C$:Mg/Ca analyses were performed on shells from a narrow range of shell sizes (300-355 μm) to minimize size-dependent variation in our $\delta^{13}C$ dataset.

2.2. Paired *in situ* $\delta^{13}C$ and Mg/Ca Microanalyses

Planktic foraminifer shells were cast with 3 grains of UWC-3 calcite standard (Kozdon et al., 2009) in the center of a 25 mm round epoxy mount, ground to the level of best exposure, polished, cleaned, and Au-coated. Prior to geochemical analysis, shells were examined by Scanning Electron Microscopy (SEM) to identify subdomains suitable for in-situ $\delta^{13}C$ and Mg/Ca ratio measurements and to avoid zones that had experienced significant diagenetic alteration within each shell (e.g., Kozdon et al., 2011). In-situ $\delta^{13}C$ measurements were performed with ~7 μm beam spot size in the WiscSIMS Laboratory at UW-Madison by a CAMECA ims-1280 large radius multicollector ion microprobe (Kita et al., 2009; Valley and Kita, 2009) using the protocols described in a previous study (Kozdon et al., 2018). The in-situ $\delta^{13}C$ microanalyses primarily targeted subdomains located at the base of pustular outgrowths (muricae) within the chamber walls of each shell. Previous studies have shown that these subdomains are less susceptible to post-depositional alteration than the rest of the shell (Kozdon et al., 2011; Kozdon et al., 2013). Between one and five SIMS $\delta^{13}C$ microanalyses were performed for each shell and averaged (Table 1). Reproducibility of the individual spot analysis of UWC-3 standard ($\delta^{13}C$ = -0.91‰ V-PDB, Kozdon et al., 2011) bracketing the samples is on average 0.7‰ (± 2 SD). After SIMS analysis, the Au-coat of the sample mount was removed, and a C-coat was applied after cleaning to facilitate SEM imaging of the SIMS analysis pits and electron microprobe analysis.

In-situ Mg/Ca ratios were acquired from ~3 μm diameter spots with a slightly larger interaction volume using a CAMECA SX-51 electron microprobe housed in the Cameron and Wilcox Microbeam Laboratory at the UW-Madison Department of Geoscience. Whenever possible, Mg/Ca spot measurements were placed adjacent to the SIMS $\delta^{13}C$ pits or in comparable subdomains within the chamber wall of each shell. Depending on the number of suitable targets for analysis, between one to five in-situ Mg/Ca measurements were performed for each shell, and the average Mg/Ca composition was calculated (Table 1). Fully quantitative microanalyses (mineral standards, background subtracted, and matrix corrected) were performed using Probe for EPMA software (Probe Software, Inc.). The natural carbonate standards Delight Dolomite and Callender Calcite were used for Mg and Ca, respectively. Mg-Kα X-rays were measured on two spectrometers and aggregated. Carbon was calculated within the matrix correction, being allocated as one atom of carbon to 3 atoms of oxygen, and oxygen by stoichiometry to the cations measured, thus analytical totals of 98 – 100.5 wt. % are a measure of accuracy. Measurements featuring analytical totals below 98 wt. % or above 100.5 wt. % were excluded from the data set.

2.3. Mg/Ca Paleotemperature Calculations

Absolute Mg/Ca-based paleotemperatures were calculated using the following equation of Hines et al. (2017):

$$T = \ln\left(\frac{[Mg/Ca_{shell}] \times [Mg/Ca_{sw}^{t=0}]^{H}}{B \times [Mg/Ca_{sw}^{t=1}]^{H}}\right) \times \frac{1}{A} \quad (1)$$

where Mg/Ca_{shell} is the measured Mg/Ca ratio (in mmol/mol), Mg/Ca_{sw} (t=0) modern seawater Mg/Ca (5.17 mol/mol), Mg/Ca_{sw} (t=1) early Eocene seawater Mg/Ca (1.6 mol/mol, Evans and Müller, 2012), A (0.09) and B (0.38) are species specific calibration constants (Anand et al., 2003), and H the power component, which relates the sensitivity of the calibration to the Mg/Ca ratio of the Eocene ocean. The H value calculated for Paleogene planktic foraminifers is lower than that of modern taxa due to differences in the Mg/Ca-temperature calibration, the Mg partitioning coefficient of calcite (D_{Mg}), and Paleogene seawater Mg/Ca_{sw} (Hines et al., 2017). We use the H value of 0.15 for *Morozovella* spp. calculated by Hines et al. (2017). A drop in pH of 0.3 units was calculated from the boron isotopic composition of planktic foraminifers from ODP Site 1209 (Penman et al., 2014) and is associated with the massive input of carbon into the ocean-atmosphere system after the CIE onset. This decrease in surface ocean pH could have resulted in an increase in foraminifer Mg/Ca. Therefore, the Mg/Ca ratios of CIE shells calcified during the

PETM (0 to 100 ka relative to the CIE onset in Table 1) were adjusted by subtracting 15% of their initial value, using the approach of Evans et al. (2015).

Published planktic foraminifer Mg/Ca ratios measured from pooled, multi-shell samples for the PETM records recovered at ODP Site 1209 atop Shatsky Rise in the North Pacific (Zachos et al., 2003, Fig. 4) and Site 865 (Tripati and Elderfield, 2004, Fig 3B) were converted to absolute temperatures using the same approach, including an adjustment for the decrease in pH after the CIE onset, to ensure comparability with our new temperature reconstruction. The PETM was associated with a significant perturbation of the global hydrological cycle with an increase in meridional transport of atmospheric water vapor (e.g., Huber and Goldner, 2012; Kozdon et al., 2020; Pagani et al., 2006; Pierrehumbert, 2002), which may have led to spatiotemporal changes in sea-surface salinity (SSS). However, we did not adjust Mg/Ca ratios for changes in SSS, as this effect is relatively minor with a reported Mg/Ca-based temperature overestimate of ~1ºC per 2 PSU salinity increase (Hönisch et al., 2013; Kısakürek et al., 2008). Pre-PETM conditions at Site 865 were calculated based on the averaged Mg/Ca ratios measured in *M. velascoensis* shells featuring pre-CIE $\delta^{13}C$ values from the 8 core samples taken from below the stratigraphic level of the CIE onset, ranging from –216 ka to –11 ka before CIE onset (Table 1).

3. Results

Due to the labor-intensive nature of sample preparation, only 25 morozovellid shells were individually analyzed via both SIMS and EPMA analyses (Table 1). Of these, 14 *M. velascoensis* shells taken from 8 samples below the established core depth (103.00 mbsf) of the CIE onset (Bralower et al., 1995) were analyzed to characterize pre-PETM, background conditions. SIMS measurements carried out on these *M. velascoensis* shells show that all 14 shells registered non-CIE $\delta^{13}C$ values (3.2 – 6.2‰ vs. V-PDB) (Fig. 2). Six additional shells (4 *M. velascoensis*, 2 *M. allisonensis*) were taken from three samples within the CIE interval. The distribution of SIMS-based $\delta^{13}C$ values for these six shells is bimodal (Fig. 2), with three of the *M. velascoensis* shells yielding non-CIE values (3.9 – 5.1‰ vs. V-PDB) and the other three shells (1 *M. velascoensis*, 2 *M. allisonensis*) registering CIE values (-0.1 – 0.8‰ vs. V-PDB). The three *M. velascoensis* shells with non-CIE $\delta^{13}C$ values are designated as reworked contaminants. Another five *M. velascoensis* shells were taken from four samples within the overlying post-CIE interval, all of which registered non-CIE $\delta^{13}C$ values (3.6 – 4.9‰ vs. V-PDB).

A total of 60 in-situ Mg/Ca measurements were performed in the 25 morozovellid shells taken from the Site 865 study section. Similar to $\delta^{13}C$, the per-shell mean Mg/Ca ratios appear to represent two separate groups, one consisting of non-CIE shells with lower values (~2.8 – 5.3 mmol/mol) and another composed of CIE shells with higher values (>7 mmol/mol) that have not been pH corrected (Fig. 2). Lowering the

Mg/Ca ratios measured in CIE shells by 15% to compensate for a drop in seawater pH increases overlap between the distributions of Mg/Ca ratios measured in non-CIE (mean = 3.82 ± 1.97 mmol/mol, 2 SD) and CIE (mean = 6.43 ± 2.73 mmol/mol, 2 SD) shells. Recent studies (John et al., 2023; Staudigel et al., 2022) that employed a smaller EPMA beam diameter facilitating a higher spatial resolution have shown that well-preserved (glassy) morozovellid shells feature significant intra-shell Mg/Ca variation expressed as micrometer-scale bands that alternate between low (~1.5 mmol/mol) and high (~13 mmol/mol) Mg/Ca ratios. A frequency histogram for all 60 in-situ Mg/Ca ratios shows that our data have a non-normal distribution with positive skewness and that variability (2.8 – 9.42 mmol/mol) approaches the reported range (John et al., 2023) of intra-shell variation for individual, glassy morozovellid shells (Fig. 3A). In addition, the only *M. velascoensis* shell registering an anomalously low $\delta^{13}C$ value also features significant intra-shell Mg/Ca variation (4.78 – 9.42 mmol/mol after pH correction) and the highest measured Mg/Ca ratio in the entire dataset (Figs. 3A). These observations raise the possibility that the higher Mg/Ca ratios measured in CIE shells is an artifact of sampling highly variable intra-shell Mg/Ca ratios. To test this null hypothesis, we segregated the Mg/Ca ratios measured in non-CIE shells (Fig. 3B) from the pH-corrected Mg/Ca ratios measured in CIE shells (Fig. 3C) and ran an unpaired Wilcoxon rank-sum test (R statistical software package, R. Core Team, 2021) on the data. This non-parametric test indicates that the likelihood of drawing the two differing Mg/Ca distributions from the same statistical population is extremely low (p-value = 1.12×10^{-5}). We therefore reject the null hypothesis and consider the difference between the non-CIE and CIE Mg/Ca distributions to be significant.

A record showing the mean Mg/Ca ratio of each shell plotted against core depth is provided in Figure 4A. All 14 of the *M. velascoensis* shells taken from below the CIE onset returned pre-CIE $\delta^{13}C$ values and per-shell Mg/Ca ratios ranging between 2.84 and 5.01 mmol/mol. Of the six shells taken from within the CIE interval, the three reworked (non-CIE) *M. velascoensis* shells register per-shell Mg/Ca ratios (3.24 – 4.60 mmol/mol) comparable to those returned by the 14 *M. velascoensis* shells from the underlying pre-CIE interval, whereas the pH-corrected per-shell Mg/Ca ratios of the three CIE shells (6.2 – 6.5 mmol/mol) are appreciably higher. As previously noted, the lone CIE shell assigned to *M. velascoensis* features significant intra-shell Mg/Ca variability (Fig. 4A). Excluding this particular *M. velascoensis* shell from the dataset has no notable effect on our Mg/Ca record, as the mean value for the CIE Mg/Ca ratios acquired from the two *M. allisonensis* shells (6.42 mmol/mol) is still relatively high. Per-shell Mg/Ca ratios for the five non-CIE *M. velascoensis* shells taken from the overlying post-CIE interval (2.79 – 5.32 mmol/mol) are similar to those recorded by the pre-CIE shells of *M. velascoensis* from below the CIE interval (Fig. 4A).

For comparison, published (Tripati and Elderfield, 2004) planktic foraminifer Mg/Ca ratios measured by ICP-OES analyses of pooled, multi-shell samples spanning the CIE interval in the same Site 865C PETM record are plotted with the per-sample mean Mg/Ca ratios that we acquired using in-situ EPMA measurements (Fig. 4B). This comparison reveals major discrepancies between the two parallel Mg/Ca ratio records. Inter-sample variability is muted and the highest Mg/Ca ratios (~4.7 mmol/mol) are registered well above the CIE interval at ~101.70 mbsf in the multi-shell record. Thus, the sharp increase in Mg/Ca ratios associated with the CIE interval and subsequent return to lower background Mg/Ca ratios over the post-CIE interval seen in our in-situ Mg/Ca record are not expressed in the Mg/Ca record constructed with multi-shell samples (Fig. 4B). Moreover, application of the pH correction to the "PETM" Mg/Ca ratios in the multi-shell record gives the impression that Mg/Ca ratios decreased over the CIE interval. Another discrepancy involves an outlier in our Mg/Ca record located just above the CIE recovery interval at 102 mbsf (Fig. 4B, asterisk). The Mg/Ca ratio for this single non-CIE shell is based on only one in-situ measurement and is therefore considered less robust.

The conversion of our in-situ Mg/Ca ratios to temperatures using Equation 1 and methods described above (section 2.3) shows that SSTs at equatorial Site 865 varied between ~24 and 30.6ºC (mean = 27.7ºC) prior to the PETM (Fig. 4B). These background SSTs were calculated using non-CIE *M. velascoensis* shells calcified prior to the CIE onset with higher $\delta^{13}C$ values and are similar to pre-CIE SSTs (mean = 28ºC) registered by the parallel series of multi-shell (*M. velascoensis*) samples. By contrast, in-situ Mg/Ca ratios for the three shells with CIE $\delta^{13}C$ values (2 *M. allisonensis*, 1 *M. velascoensis*) yield SSTs between 33-34ºC, whilst the multi-shell record shows little, to no, temperature change over the CIE interval. Finally, Mg/Ca ratios for the five non-CIE *M. velascoensis* shells from the overlying post-CIE interval yield relatively cooler SSTs (mean = 27.3ºC) ranging between 24ºC and 31.3ºC (Fig. 4B). The post-CIE cooling delineated by our in-situ Mg/Ca record contrasts starkly with the modest degree of post-CIE warming seen in the multi-shell record. In summation, our $\delta^{13}C$ filtered Mg/Ca record suggests that tropical SSTs reached 33 to 34°C at equatorial Site 865 during the PETM, about 6°C above pre-PETM background conditions, while the Mg/Ca-based SST record constructed with samples consisting of pooled, multiple *M. velascoensis* shells suggests no tropical warming during the PETM (Fig. 4B).

4. Discussion

4.1. Site 865 SST Record for the PETM

Our planktic foraminifer Mg/Ca-derived temperature record indicates that tropical SSTs increased by ~6ºC above background temperatures during the PETM, with SSTs reaching 33 to 34ºC at equatorial Site 865 (Fig. 4B). These PETM SSTs are significantly warmer than tropical temperatures observed in the modern ocean that rarely exceed 30°C (e.g., Huber and Sloan, 2001). The method of $\delta^{13}C$ isotopic filtering made it possible to identify reworked non-CIE shells within the critical CIE interval of Site 865, which we omitted from our SST record for the PETM (Fig. 2). Due to their lower Mg/Ca ratios, the inclusion of such non-CIE shells would have led to an underestimation of tropical SSTs for the PETM. This is especially true for the Site 865 PETM record where previous $\delta^{13}C$ isotopic filtering of planktic foraminifer assemblages showed that roughly half of all specimens within the CIE interval are reworked, non-CIE contaminants (Hupp et al., 2022).

The deleterious effects of this sediment mixing are demonstrated through comparison of our $\delta^{13}C$ filtered Mg/Ca record to a published (Tripati and Elderfield, 2004) Mg/Ca record constructed with pooled, multi-shell samples for the same Site 865C PETM section (Fig. 4B). Comparison of these two parallel records reveals several glaring inconsistencies, which seems odd since similar parallel Mg/Ca records constructed with EPMA in-situ measurements inside individual planktic foraminifer shells and ICP-MS analyses of multi-shell samples yielded nearly identical SST trends and Mg/Ca ratios across the PETM record of ODP Site 690 in the Weddell Sea (Kozdon et al., 2020). Be that as it may, Mg/Ca ratios in the multi-shell record appear relatively invariant compared to the inter-sample variability in our in-situ Mg/Ca record over the pre-CIE interval at Site 865. This discrepancy could be an indication that the limited number of per-shell Mg/Ca ratios in our in-situ record does not capture the full range of inter-shell Mg/Ca variability in each sample, which would cause the resulting per-sample Mg/Ca ratios to fluctuate in the in-situ record. Alternatively, inter-sample variability in the multi-shell Mg/Ca record may have been attenuated by the smoothing effect of sediment mixing. These two explanations need not be mutually exclusive, and we note that the mean pre-PETM SST is ~28ºC in both records. This brings us to the most striking incongruency between the two records; specifically, the transient rise in tropical SSTs over the CIE interval seen in our in-situ Mg/Ca record is completely missing in the multi-shell Mg/Ca record (Fig. 4B). This disparity is clearly an artifact of sediment mixing in the Mg/Ca record constructed with multi-shell samples. By contrast, screening of planktic foraminifer shells on the basis of their $\delta^{13}C$ compositions and the exclusion of non-CIE shells from the critical CIE interval facilitates the extraction of a much cleaner signal of PETM warming from the in-situ Mg/Ca-based SST record. The divergence between the two parallel Mg/Ca records over the post-CIE interval where the warmest SSTs (~29ºC) in the multi-shell record are registered whilst our in-situ Mg/Ca record shows rapid cooling in the aftermath of the PETM is puzzling (Fig. 4B). One possibility is that non-CIE shells from the very tail end of the PETM recovery when SSTs were still relatively warmer were displaced upwards in the stratigraphic record, as suggested by the lone non-CIE shell that yielded a relatively high Mg/Ca ratio at 102.00 mbsf in our in-situ record (Fig. 4B). The cause of divergence between the two Mg/Ca records across the post-CIE interval remains unclear, but we emphasize that the cooling of SSTs over the post-CIE interval in our in-situ Mg/Ca record is also seen in most other open-ocean PETM records (e.g., Kennett Bains et al., 2000; Kennett and Stott, 1991; Kozdon et al., 2020; Zachos et al., 2003).

The implications of a ~6°C rise in tropical SSTs during the PETM are far-reaching. According to modeling studies (e.g., Huber and Caballero, 2011), an abrupt and extreme increase in greenhouse gas levels should give rise to warming at all latitudes. Yet, the majority of published temperature records indicate a relatively modest (~3°C) warming of the tropics (e.g., Dunkley Jones et al., 2013; Frieling et al., 2017) and a more pronounced temperature increase of 5-8°C at mid- and high-latitude regions (Kennett and Stott, 1991; Sluijs et al., 2006; Sluijs et al., 2011; Zachos et al., 2006). Taken at face value, a compilation of published SST records from across tropical and temperate paleolatitudes (31º S to 38º N) suggests a reduction in meridional temperature gradients during the PETM (Fig. 5), which has raised questions regarding the extent to which PETM warming was amplified at high-latitude, polar regions (e.g., Inglis et al., 2020; Tierney et al., 2022). However, the ~6°C warming of tropical SSTs during the PETM inferred from our new pelagic Mg/Ca-based SST record indicates that PETM warming was more uniformly distributed across the latitudes, so tropical-to-temperate latitudinal temperature gradients may not have been as low as some foraminifer-based proxy ($\delta^{18}O$, Mg/Ca) records suggest (Fig. 5).

Other than a single $\delta^{18}O$ record constructed with well-preserved, glassy planktic foraminifer shells from a tropical PETM section in Tanzania (Aze et al., 2014), planktic foraminifer-based $\delta^{18}O$ and Mg/Ca paleorecords suggest tropical SSTs were at least 4ºC cooler than those herein reported for the PETM (Fig. 5). Furthermore, the magnitude of PETM warming expressed by many of these published planktic foraminifer-based records (3-4°C) is less than the ~6°C warming inferred from our new Site 865 Mg/Ca record, a possible exception is the ~8ºC warming returned by the planktic foraminifer $\delta^{18}O$ record for a coastal PETM section at Wilson Lake, New Jersey (Fig. 5). Interestingly, the magnitude of PETM warming inferred from our new 'isotopically-filtered' Mg/Ca record is more congruent with that registered by SST records constructed with the organic TEX_{86} biomarker proxy (Frieling et al., 2017; Sluijs et al., 2007). Still, our tropical SST record does not yield the exceptionally warm temperatures (>35ºC) captured by the aforementioned studies using glassy planktic foraminifer shells preserved in hemipelagic sediments from Tanzania (Aze et al., 2014) and TEX_{86} analyses of shelf sediments deposited in Nigeria (Frieling et al., 2017).

4.2. Omission of Peak Tropical Warming due to "Thermal Blackout"?

There are reasons to suspect that our Mg/Ca-based SST record may not capture peak tropical SSTs at equatorial Site 865 during the PETM. The first involves shoaling of the carbonate compensation depth in response to rapid carbon input during the earliest stages of the PETM (e.g., Dickens et al., 1997; Zeebe et al., 2009). This initial pulse of pervasive carbonate dissolution manifests as a drop in sedimentary calcite ($CaCO_3$) content and a clay-rich dissolution layer at the base of most deep-sea PETM records (e.g., Bralower et al., 2014; Kelly et al., 2010; Thomas et al., 1999; Zachos et al., 2003; 2005). A distinctive clay-rich dissolution layer is not present in the Site 865 PETM record, but an absence of lithological change across the CIE onset does not rule out the possibility that the base of this PETM stratigraphy is punctuated by a brief hiatus. The abrupt nature of the CIE onset and lack of intermediate values in single-shell foraminifer $\delta^{13}C$ records is consistent with the view that the base of the Site 865 PETM record has been truncated by carbonate dissolution (Hupp et al., 2022; Kelly et al., 1996). This being the case, then the absence of a clay-rich dissolution layer may simply be due to the vast geographic distance separating pelagic Site 865 from any major source of terrestrial (eolian) input from the continents. Thus, SST reconstructions based on foraminifer calcite may not record peak warming during the earliest stages of the PETM when carbonate dissolution was most intense.

It has also been proposed that thermal stress wrought by PETM conditions may have exceeded the upper temperature tolerances of many tropical marine plankton (Aze et al., 2014; Frieling et al., 2017). In fact, heat stress has been shown to be the principal driver for major shifts in the biogeographic ranges of calcareous phytoplankton during the PETM (Gibbs et al., 2016). Further, $\delta^{13}C$ isotopic filtering of planktic foraminifer assemblages has shown that local diversity and population dynamics were profoundly perturbed by PETM conditions at Site 865 (Hupp et al., 2022). For instance, $\delta^{13}C$ isotopic filtering of planktic foraminifers on a per-taxon basis shows that despite having continuous (uninterrupted) stratigraphic ranges across the CIE interval, none of the shells belonging to the mixed layer-dwelling *Morozovella aequa*-*M. subbotinae* group and thermocline-dwelling genus *Subbotina* spp. recorded CIE $\delta^{13}C$ values. This realization indicates that local populations of these two taxa were extirpated by PETM conditions at Site 865, even though their fossil records suggest otherwise (Hupp et al., 2022). Furthermore, unlike their benthic counterparts, planktic foraminifers did not experience a major extinction event during the PETM, as many of the species that suffered local extinctions subsequently repopulated the tropics (Hupp et al., 2022). Such transitory fluctuations in local population dynamics are thought to reflect a short-lived episode of ecological exclusion, where species initially emigrate out of the tropics due to excessive heat stress only to immigrate back into the tropics as extreme PETM warming waned (Aze et al., 2014; Hupp et al., 2022). We therefore posit that the combined effects of upward displacement of pre-CIE shells into the overlying CIE interval followed by the renewed deposition of shells during the ensuing recolonization phase conspired to obscure the record of ephemeral extratropical migrations undertaken by many planktic foraminifer species, including *M. velascoensis*, in the Site 865 PETM sedimentary archive (Hupp et al., 2022; Kelly et al., 1998).

When viewed through the lens of thermally-induced ecological exclusion, the possibility that all planktic foraminifers temporarily emigrated out of the Site 865 study area to escape extreme PETM warmth cannot be ruled out. Credence is lent to this interpretation by the comprehensive work of Bijma et al. (1990), which showed that such vital physiological processes as food acceptance, growth, calcification and reproduction are all inhibited in modern tropical planktic foraminifers at water temperatures centered on ~32ºC. Hence, the SSTs registered by our 'unmixed' Mg/Ca-based temperature record for the PETM (~33-34ºC) meet, or even exceed, the maximum temperature tolerances of modern planktic foraminifer species. An important corollary is that periods of peak PETM warmth at pelagic Site 865 and other tropical sites may not be captured by planktic foraminifer shells, as even species featuring the highest heat tolerance such as the morozovellids may have temporarily evacuated tropical regions due to overwhelming thermal stress. Such a tropical exodus of planktic foraminifers would result in a 'thermal blackout' where peak PETM SSTs in tropical settings such as Site 865 are not recorded (*sensu* Aze et al., 2014). The record of such a short-lived omission (i.e. thermal blackout) to tropical PETM records from pelagic settings would subsequently be obscured by sediment mixing and/or the pulse of CO_2-induced carbonate dissolution fueled by carbon input during the PETM (Zachos et al., 2005; Zeebe et al., 2009; Zhang et al., 2020).

4.3. Mg/Ca of Diagenetic Calcite

Inorganic precipitation experiments suggest that the Mg-content of diagenetic calcite is about an order of magnitude higher than the Mg-content of the biogenic calcite formed by planktic foraminifers at the same temperature (Mucci, 1987; Oomori et al., 1987). Thus, it is intuitive to assume that the contribution of diagenetic calcite may bias Mg/Ca-based PETM paleorecords towards higher temperatures. However, this assumption is at odds with the vast majority of Mg/Ca-based paleorecords from the tropical realm indicating relatively 'cool' temperatures for Paleogene hyperthermal climate states that are difficult to reproduce with climate model simulations (e.g. Lunt et al., 2016; Lunt et al., 2017). Additionally, recent studies suggest that, depending on the diagenetic setting, the Mg-content of inorganically-formed calcite can be equal to, or even lower, than the biogenic calcite formed by planktic foraminifers. Kozdon et al. (2013) reported the Mg/Ca ratios of diagenetic crystallites from near the base of the Site 865 PETM record that approach those of planktic foraminifer shells. More recently, Lammers and Mitnick (2019) measured the Mg/Ca ratios of late Eocene inorganic calcites from ODP Site 807 (Ontong Java Plateau) and found values significantly lower than those measured in planktic foraminifer shells. This finding suggests that, at typical bottom-water temperatures, the equilibrium Mg-distribution coefficient is at least one order of magnitude lower than values previously inferred from inorganic calcite precipitation experiments (Lammers and Mitnick, 2019). Thus, recent research indicates a strong possibility that similar to $\delta^{18}O$, diagenesis may bias Mg/Ca-based paleorecords toward lower temperatures under some diagenetic settings.

Finally, we emphasize that the veracity of our Mg/Ca-based SST record is further enhanced by the in-situ measurement of Mg/Ca ratios in isolated subdomains within individual planktic foraminifer shells, and that these subdomains are homologous to the relatively well-preserved subdomains of planktic foraminifer shells from the same Site 865 PETM record that yielded relatively low $\delta^{18}O$ values (–3‰ to -4‰ V-PDB) indicative of biogenic calcite (Kozdon et al., 2011, 2013). In other words, the microanalytical techniques used for this study make it possible to perform in-situ $\delta^{13}C$ and Mg/Ca measurements on isolated subdomains that are better preserved than the rest of the shell, thereby avoiding other parts of the same shell that may have been more strongly altered by carbonate diagenesis (Kozdon et al., 2011, 2013). Furthermore, partial recrystallization of planktic foraminifer shells much like those used in this study acts as a "closed system" that reduces intra-shell Mg/Ca variability without significantly altering the bulk-shell Mg/Ca composition (Staudigel et al., 2022). This diagenetic process likely decreased intra-shell Mg/Ca variation in the partially recrystallized (frosty) morozovellid shells we targeted for in-situ Mg/Ca analyses, which further improved the fidelity of our Mg/Ca-based SST record. We therefore consider the effects of diagenetic overprinting on our Mg/Ca-based temperature record to be negligible and posit that tropical SSTs (~33-34ºC) likely exceeded the maximum thermal tolerances of planktic foraminifers during the PETM.

5. Conclusions

Paired in-situ $\delta^{13}C$:Mg/Ca analyses within subdomains of the same individual planktic foraminifer shells are used to reconstruct change in tropical SSTs during the PETM at pelagic Site 865 in the central Pacific Ocean. A method referred to as 'isotopic filtering' was used to differentiate foraminifer shells featuring CIE and non-CIE $\delta^{13}C$ values and subsequently omit reworked, non-CIE shells from our Mg/Ca-based SST record for the PETM. The exclusion of non-CIE shells with lower Mg/Ca ratios enhanced the fidelity of our SST record, which in turn revealed that the SSTs increased by ~6ºC relative to pre-PETM conditions at this tropical site, with SSTs reaching 33-34ºC during the during the PETM. This temperature anomaly is about twice as high as suggested by previously published paleorecords from pelagic sites and approximates the magnitude of warming reported from the extratropical realm, indicating that latitudinal temperature gradients with less pronounced polar amplification may have been maintained during the PETM.

Our $\delta^{13}C$ filtered, Mg/Ca ratio record for the PETM does not register tropical SSTs >34°C as reported by some studies; however, our temperature record reflects open ocean conditions that may not be comparable to the shelf and hemipelagic settings from where these extreme tropical temperatures were recorded. Furthermore, we posit that thermal stress wrought by PETM conditions exceeded the upper temperature tolerances of planktic foraminifers (Aze et al., 2014; Frieling et al., 2017), which triggered a short-lived extratropical migration of many species followed by their return to equatorial Site 865 as peak PETM conditions waned. Such a transient tropical exodus would result in a brief "thermal blackout" in our planktic foraminifer Mg/Ca-based SST record, thus peak PETM temperatures (>34ºC) at Site 865 may not be captured by our SST record. In addition, increased carbonate dissolution fueled by the rapid release of massive amounts of carbon into the ocean-atmosphere system likely truncated the base of the PETM record, which may have removed the earliest stages of PETM warming. Regardless, our $\delta^{13}C$ filtered Mg/Ca-based SST record provides a thermal benchmark for constraining the effects of PETM warming on tropical plankton communities inhabiting the pelagic realm.

Conflict of Interest

The authors declare no conflicts of interest relevant to this study.

Open Research

The $\delta^{13}C$ and Mg/Ca data used for this study are summarized in Table 1. Detailed data tables (individual $\delta^{13}C$ and Mg/Ca measurements) are archived in the repository of the PANGAEA Data Publisher and available as .tab and html format at Kozdon and Kelly (2024a; b; c; d).

Acknowledgements

This research used samples provided by the International Ocean Discovery Program (IODP). Funding for this research courtesy NSF-OCE 1405224 to D.C.K and R.K. WiscSIMS is supported by NSF (EAR 2004618) and UW – Madison. John Fournelle assisted with Mg/Ca ratio measurements by EPMA. We thank Seth Sutton (UW-Madison) for performing the statistical analyses using the R statistical package.

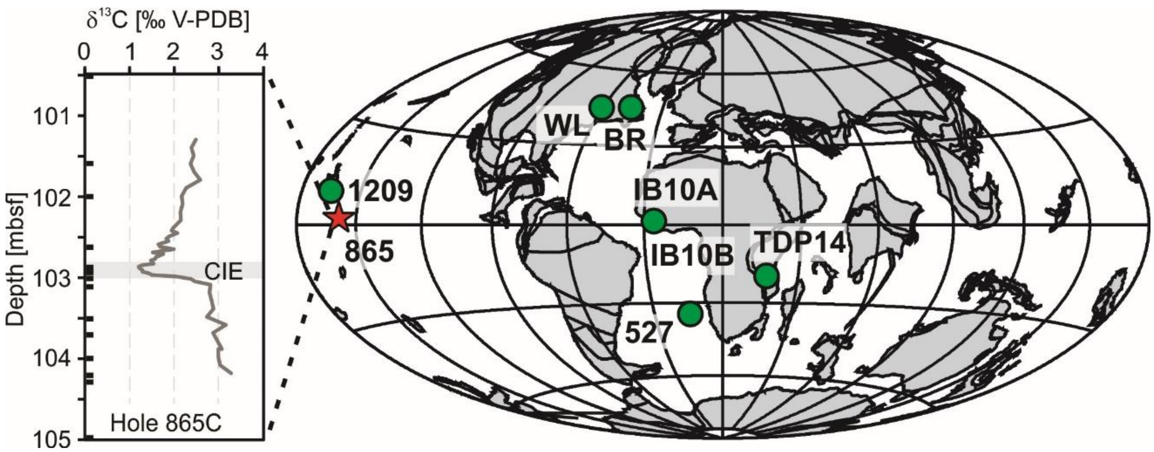

Figure 1. Right: Map showing early Eocene paleogeography (from the Ocean Drilling Stratigraphic Network, ODSN, http://www.odsn.de/) and locations of all sites referred to in this study. Red star demarcates equatorial location of PETM study section (ODP Site 865) used to compile a paired $\delta^{13}C$:Mg/Ca record. **Left**: Bulk-carbonate $\delta^{13}C$ record of the CIE in the Site 865 PETM section (Hupp et al., 2022). Light gray shading delimits the lower part of the CIE interval. Black tick marks along vertical axis indicate core depths of samples used in this study.

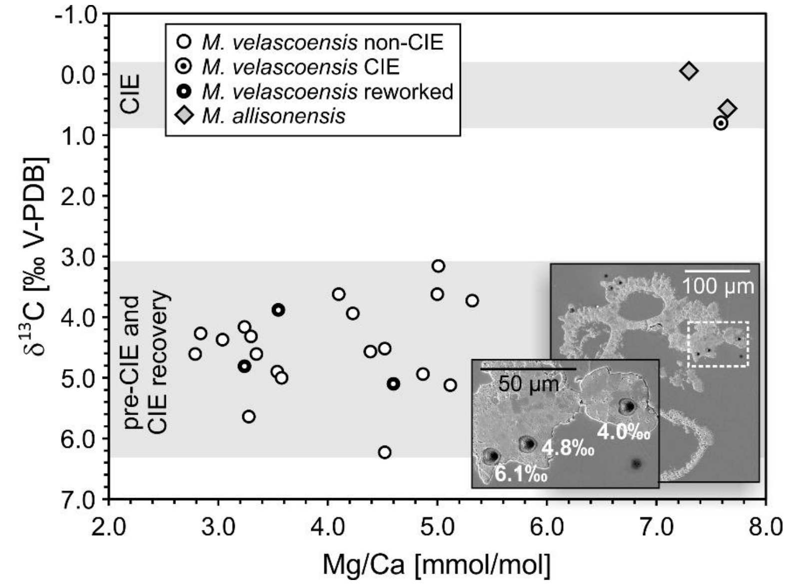

Figure 2. Cross plot showing pairwise comparison of the mean $\delta^{13}C$ composition and Mg/Ca ratio of each planktic foraminifer shell from the Site 865 study section. All geochemical data acquired using in-situ measurements within individual shells belonging to the species *M. velascoensis* and the PETM morphotype *M. allisonensis*. Non-CIE shells feature relatively high $\delta^{13}C$ values (3.2 – 6.2 ‰) and low Mg/Ca ratios (2.8 – 5.3 mmol/mol), whereas CIE shells calcified during PETM feature relatively low $\delta^{13}C$ values (-0.1 – 0.8 ‰) and high Mg/Ca ratios (>7 mmol/mol, shown without pH correction). Reworked *M. velascoensis* are shells with non-CIE $\delta^{13}C$ values from within the CIE interval. Inserted images show same *M. velascoensis* shell, polished to midsection, with ~7 µm pits for *in situ* $\delta^{13}C$ measurements. White dashed box delimits more highly magnified part of shell with $\delta^{13}C$ values (white numbers). Mg/Ca analyses (not visible) were placed in comparable subdomains.

489

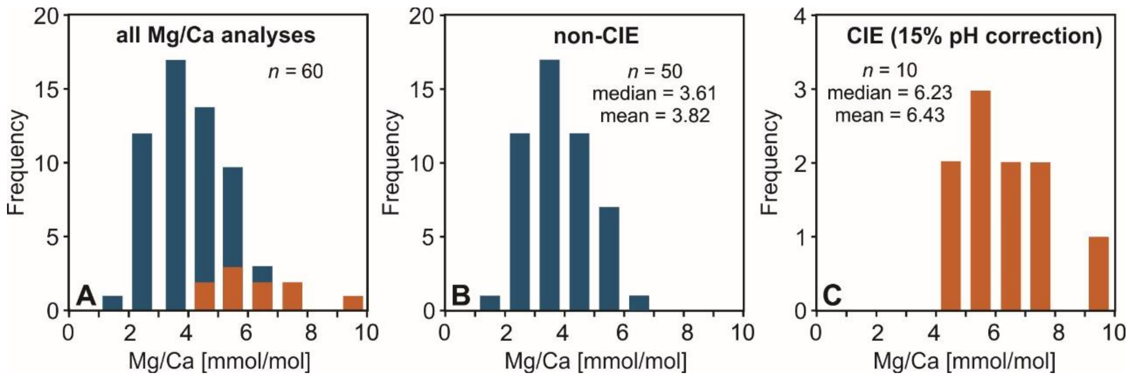

Figure 3. Comparison of frequency distributions for planktic foraminifer Mg/Ca ratios compiled in this study from the Site 865 PETM record. **(A)** Histogram showing positively skewed distribution of all 60 in-situ Mg/Ca measurements in non-CIE (blue) and CIE (orange) shells (median = 4.03 mmol/mol). (**B**) Histogram showing positively skewed distribution of 50 in-situ Mg/Ca measurements in non-CIE shells (median = 3.61 mmol/mol). **(C)** Histogram showing positively skewed distribution of 10 in-situ, pH-corrected Mg/Ca measurements in CIE shells (median = 6.23 mmol/mol).

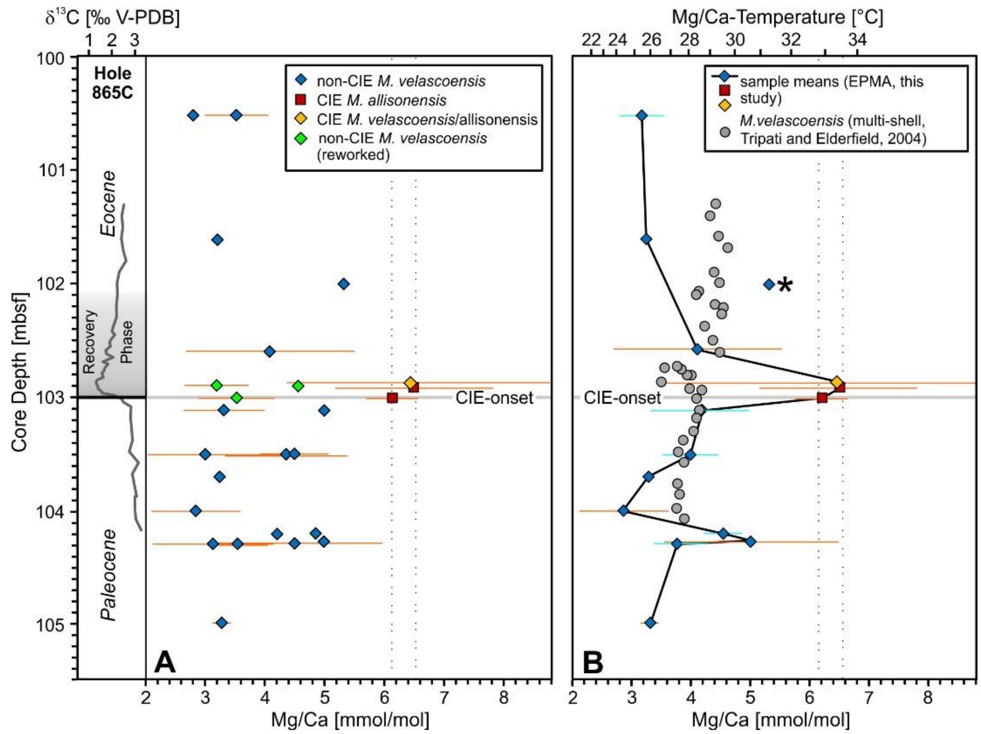

Figure 4. (A) Per-shell Mg/Ca ratios of *M. velascoensis* and the PETM morphotype *M. allisonensis* acquired in-situ by EPMA plotted versus core depth. Reworked shells (based on their $\delta^{13}C$ composition) within CIE interval are denoted by green diamonds. Each data point connotes the average of 1-5 in-situ analyses per shell. Orange error bars represent ±1 SD as determined by the intra-shell variability in Mg/Ca. Bulk-carbonate $\delta^{13}C$ record (Hupp et al., 2022) delineating the CIE onset and subsequent recovery phase in Site 865C PETM section is shown on the far left. (**B**) Per-sample mean Mg/Ca ratios plotted against core depth and converted to Mg/Ca-based SSTs. Mg/Ca ratios of reworked shells within the CIE interval excluded from SST calculations. A correction was applied to Mg/Ca ratios (-15%) for CIE shells (red squares, yellow diamond) to account for lower ocean pH during PETM. SST curve (solid line) constructed with mean Mg/Ca ratios for each sample. Blue error bars represent ± 1 standard error of the mean for samples with multiple per-shell Mg/Ca ratios. Orange error bars ±1 SD for samples with only one shell. The data point marked by asterisk is based on a single EPMA measurement and considered less robust. A planktic foraminifer Mg/Ca ratio record based on multi-shell (*M. velascoensis*) samples for the Site 865C PETM section (Tripati and Elderfield, 2004) is shown for comparison (gray filled circles), with same pH correction applied to values measured from the CIE interval.

492

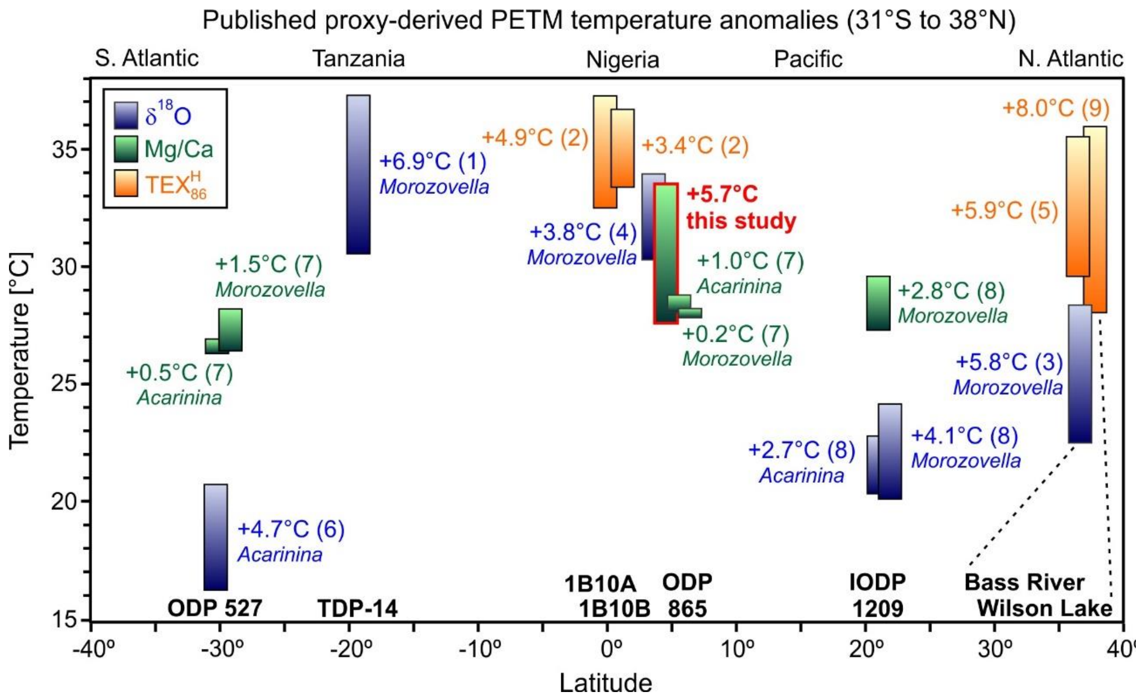

Figure 5. Comparison of published PETM temperature anomalies (Δ*T* from pre-PETM to peak-PETM) for several tropical and subtropical sites plotted vs. paleolatitudes ranging from 31.1°S to 38.2°N. Blue and green bars: SSTs calculated from the $\delta^{18}O$ or Mg/Ca composition of planktic foraminifers, respectively. Orange bars: TEX_{86}^{H}-based SST reconstructions. References: (1) Aze et al. (2014), (2) Frieling et al. (2017), (3) John et al. (2008), (4) Kozdon et al,. (2011), (5) Sluijs et al. (2007), (6) Thomas et al. (1999), (7) Tripati and Elderfield (2004), (8) Zachos et al. (2003), (9) Zachos et al., (2006). The Mg/Ca ratios from references 7 and 8 were converted to SSTs using the same approach as for the in-situ Mg/Ca data reported in this study. TEX_{86}^{H} and $\delta^{18}O$-based paleotemperatures have been previously (re-)calculated by Frieling et al. (2017) using consistent methods to allow for a direct comparison.

Table 1. Paired $\delta^{13}C$:Mg/Ca measurements and calculated SSTs for individual planktic foraminifer shells from the Site 865 PETM record. In-situ measurements for $\delta^{13}C$ and Mg/Ca performed using SIMS and EPMA, respectively.

Hole, Core Section, Interval [cm]	Core depth [mbsf]	Age rel. CIE onset [ka]	Species	$\delta^{13}C$ shell avg. [‰ V-PDB]	*n* $\delta^{13}C$	Mg/Ca shell avg. [mmol/mol]	*n* Mg/Ca	Mg/Ca SST [ºC]
865C 12-2, 70-72	100.50	439	*M. velascoensis*	4.90	3	3.54	3	26.8
865C 12-2, 70-72	100.50	439	*M. velascoensis*	4.61	3	2.79	1	24.1
865C 12-3 30-32	101.60	268	*M. velascoensis*	4.16	2	3.24	1	25.8
865C 12-3 70-72	102.00	206	*M. velascoensis*	3.73	2	5.32	1	31.3
865C 12-3 130-132	102.60	112	*M. velascoensis*	3.62	3	4.10	3	28.4
865C 12-4 6-8	102.87	41	*M. velascoensis*	0.80	2	7.59[*]	3	33.4
865C 12-4 10-12	102.90	31	*M. velascoensis*[#]	5.10	1	4.60	1	29.7
865C 12-4 10-12	102.90	31	*M. velascoensis*[#]	4.81	2	3.24	3	25.8
865C 12-4 10-12	102.90	31	*M. allisonensis*	0.57	3	7.65[*]	5	33.5
865C 12-4 20-22	103.00	0.0	*M. allisonensis*	-0.05	2	7.30[*]	2	33.0
865C 12-4 20-22	103.00	0.0	*M. velascoensis*[#]	3.88	2	3.55	3	26.8
865C 12-4 30-32	103.10	-11	*M. velascoensis*	3.62	3	5.00	1	30.6
865C 12-4 30-32	103.10	-11	*M. velascoensis*	4.61	2	3.55	3	26.8
865C 12-4 70-72	103.50	-54	*M. velascoensis*	4.57	1	4.39	4	29.1
865C 12-4 70-72	103.50	-54	*M. velascoensis*	4.37	5	3.04	3	25.1
865C 12-4 70-72	103.50	-54	*M. velascoensis*	4.52	3	4.52	3	29.5
865C 12-4 90-92	103.70	-75	*M. velascoensis*	5.64	1	3.28	1	25.9
865C 12-4 122-124	104.00	-108	*M. velascoensis*	4.27	4	2.84	3	24.3
865C 12-4 140-142	104.20	-129	*M. velascoensis*	3.74	3	4.23	1	28.7
865C 12-4 140-142	104.20	-129	*M. velascoensis*	4.94	2	4.87	1	30.3
865C 12-4 146-149	104.28	-138	*M. velascoensis*	3.16	1	5.01	3	30.6
865C 12-5 0-2	104.30	-140	*M. velascoensis*	5.00	4	3.58	3	26.9
865C 12-5 0-2	104.30	-140	*M. velascoensis*	6.23	4	4.52	3	29.5
865C 12-5 0-2	104.30	-140	*M. velascoensis*	5.12	4	3.18	2	25.6
865C 12-5 70-72	105.00	-216	*M. velascoensis*	4.32	5	3.30	3	26.0

Samples from the CIE interval are highlighted by light gray shading

Sample ages reported relative (±kyr) to CIE onset where CIE onset = 0.0 kyr (after Kozdon et al., 2011).

[#] Displaced shell (pre-CIE $\delta^{13}C$ composition).

[*] Measured Mg/Ca ratio, subsequently adjusted by -15% (not shown in table) to compensate for the effect of the drop in ocean pH after CIE onset on shell-Mg/Ca.

REFERENCES

Anand, P., H. Elderfield, and M. H. Conte (2003), Calibration of Mg/Ca thermometry in planktonic foraminifera from a sediment trap time series, *Paleoceanography*, *18*(2), 1050, doi:10.1029/2002pa000846.

Aze, T., et al. (2014), Extreme warming of tropical waters during the Paleocene–Eocene Thermal Maximum, *Geology*, doi:10.1130/g35637.1.

Bains, S., R. D. Norris, R. M. Corfield, and K. L. Faul (2000), Termination of global warmth at the Palaeocene/Eocene boundary through productivity feedback, *Nature*, *407*(6801), 171-174.

Berger, W., and R. Johnson (1978), On the thickness and the ^{14}C age of the mixed layer in deep-sea carbonates, *Earth Planet. Sci. Lett.*, *41*(2), 223-227.

Berger, W. H., and G. R. Heath (1968), Vertical mixing in pelagic sediments.

Bijma, J., W. W. Faber, and C. Hemleben (1990), Temperature and salinity limits for growth and survival of some planktonic foraminifers in laboratory cultures, *J. Foraminifer. Res.*, *20*(2), 95-116.

Bralower, T. J., and J. Mutterlose (1995), Calcareous nannofossil biostratigraphy of Site 865, Allison Guyot, Central Pacific Ocean: A tropical Paleogene reference section, in *Proceedings of the Ocean Drilling Program, Scientific Results*, edited by E. L. Winterer, W. W. Sager, J. V. Firth and J. M. Sinton, pp. 31-74.

Bralower, T. J., K. J. Meissner, K. Alexander, and D. J. Thomas (2014), The dynamics of global change at the Paleocene-Eocene thermal maximum: A data-model comparison, *Geochemistry, Geophysics, Geosystems*, *15*(10), 3830-3848.

Bralower, T. J., J. C. Zachos, E. Thomas, M. Parrow, C. K. Paull, D. C. Kelly, I. P. Silva, W. V. Sliter, and K. C. Lohmann (1995), Late Paleocene to Eocene paleoceanography of the equatorial Pacific Ocean: Stable isotopes recorded at Ocean Drilling Program Site 865, Allison Guyot, *Paleoceanography*, *10*(4), 841-865.

D'Hondt, S., J. C. Zachos, and G. Schultz (1994), Stable isotopic signals and photosymbiosis in Late Paleocene planktic foraminifera, *Paleobiology*, *20*(3), 391-406.

Dickens, G. R., J. R. O'Neil, D. K. Rea, and M. Owen (1995), Dissociation of oceanic methane hydrate as a cause of the carbon isotope excursion at the end of the Paleocene., *Paleoceanography*, *10*, 965-971.

Dickens, G. R., M. M. Castillo, and J. C. G. Walker (1997), A blast of gas in the latest Paleocene: Simulating first-order effects of massive dissociation of oceanic methane hydrate, *Geology*, *25*(3), 259-262, doi:10.1130/0091-7613(1997)025<0259:abogit>2.3.co;2.

Dunkley Jones, T., D. J. Lunt, D. N. Schmidt, A. Ridgwell, A. Sluijs, P. J. Valdes, and M. Maslin (2013), Climate model and proxy data constraints on ocean warming across the Paleocene–Eocene Thermal Maximum, *Earth-Sci. Rev.*, *125*, 123-145, doi:http://dx.doi.org/10.1016/j.earscirev.2013.07.004.

Evans, D., and W. Müller (2012), Deep time foraminifera Mg/Ca paleothermometry: Nonlinear correction for secular change in seawater Mg/Ca, *Paleoceanography*, *27*(4), PA4205, doi:10.1029/2012pa002315.

Evans, D., J. Erez, S. Oron, and W. Müller (2015), Mg/Ca-temperature and seawater-test chemistry relationships in the shallow-dwelling large benthic foraminifera Operculina ammonoides, *Geochimica et Cosmochimica Acta*, *148*(0), 325-342, doi:http://dx.doi.org/10.1016/j.gca.2014.09.039.

Frieling, J., H. Gebhardt, M. Huber, O. A. Adekeye, S. O. Akande, G.-J. Reichart, J. J. Middelburg, S. Schouten, and A. Sluijs (2017), Extreme warmth and heat-stressed plankton in the tropics during the Paleocene-Eocene Thermal Maximum, *Science advances*, *3*(3), e1600891.

Gibbs, S. J., P. R. Bown, A. Ridgwell, J. R. Young, A. J. Poulton, and S. A. O'Dea (2016), Ocean warming, not acidification, controlled coccolithophore response during past greenhouse climate change, *Geology*, *44*(1), 59-62.

Gutjahr, M., A. Ridgwell, P. F. Sexton, E. Anagnostou, P. N. Pearson, H. Pälike, R. D. Norris, E. Thomas, and G. L. Foster (2017), Very large release of mostly volcanic carbon during the Palaeocene-Eocene Thermal Maximum, *Nature*, *548*, 573-577.

Hines, B. R., C. J. Hollis, C. B. Atkins, J. A. Baker, H. E. Morgans, and P. C. Strong (2017), Reduction of oceanic temperature gradients in the early Eocene Southwest Pacific Ocean, *Palaeogeogr., Palaeoclimatol., Palaeoecol.*, *475*, 41-54.

Hollis, C. J., T. Dunkley Jones, E. Anagnostou, P. K. Bijl, M. J. Cramwinckel, Y. Cui, G. R. Dickens, K. M. Edgar, Y. Eley, and D. Evans (2019), The DeepMIP contribution to PMIP4: methodologies for selection, compilation and analysis of latest Paleocene and early Eocene climate proxy data, incorporating version 0.1 of the DeepMIP database, *Geoscientific Model Development Discussions*, *2019*, 1-98.

Hönisch, B., K. A. Allen, D. W. Lea, H. J. Spero, S. M. Eggins, J. Arbuszewski, P. deMenocal, Y. Rosenthal, A. D. Russell, and H. Elderfield (2013), The influence of salinity on Mg/Ca in planktic foraminifers – Evidence from cultures, core-top sediments and complementary δ18O, *Geochimica et Cosmochimica Acta*, *121*(0), 196-213, doi:http://dx.doi.org/10.1016/j.gca.2013.07.028.

Huber, M., and L. C. Sloan (2001), Heat transport, deep waters and thermal gradients: Coupled simulation of on Eocene greenhouse climate, *Geophysical Research Letters*, *28*, 3481-3484.

Huber, M. (2008), A hotter greenhouse?, *Science*, *321*(5887), 353-354.

Huber, M., and R. Caballero (2011), The early Eocene equable climate problem revisited, *Clim. Past*, *7*(2), 603-633, doi:10.5194/cp-7-603-2011.

Huber, M., and A. Goldner (2012), Eocene monsoons, *Journal of Asian Earth Sciences*, *44*(0), 3-23, doi:http://dx.doi.org/10.1016/j.jseaes.2011.09.014.

Hull, P. M., P. J. Franks, and R. D. Norris (2011), Mechanisms and models of iridium anomaly shape across the Cretaceous–Paleogene boundary, *Earth Planet. Sci. Lett.*, *301*(1-2), 98-106.

Hupp, B. N., D. C. Kelly, and J. W. Williams (2022), Isotopic filtering reveals high sensitivity of planktic calcifiers to Paleocene–Eocene thermal maximum warming and acidification, *Proceedings of the National Academy of Sciences*, *119*(9), e2115561119.

Hupp, B. N., D. C. Kelly, R. Kozdon, I. J. Orland, and J. W. Valley (2023), Secondary controls on the stratigraphic signature of the carbon isotope excursion marking the Paleocene-Eocene thermal maximum at Ocean Drilling Program Site 1135, *Chem. Geol.*, *632*, 121534.

Hutson, W. H. (1980), Bioturbation of deep-sea sediments: Oxygen isotopes and stratigraphic uncertainty, *Geology*, *8*(3), 127-130.

Inglis, G. N., F. Bragg, N. J. Burls, M. J. Cramwinckel, D. Evans, G. L. Foster, M. Huber, D. J. Lunt, N. Siler, and S. Steinig (2020), Global mean surface temperature and climate sensitivity of the early Eocene Climatic Optimum (EECO), Paleocene–Eocene Thermal Maximum (PETM), and latest Paleocene, *Climate of the Past*, *16*(5), 1953-1968.

John, C. M., S. M. Bohaty, J. C. Zachos, A. Sluijs, S. Gibbs, H. Brinkhuis, and T. J. Bralower (2008), North American continental margin records of the Paleocene-Eocene thermal maximum: Implications for global carbon and hydrological cycling, *Paleoceanography*, *23*(2), PA2217, doi:10.1029/2007pa001465.

John, E. H., P. T. Staudigel, B. Buse, C. H. Lear, P. N. Pearson, and S. M. Slater (2023), Revealing their true stripes: Mg/Ca banding in the Paleogene planktonic foraminifera genus Morozovella and implications for paleothermometry, *Paleoceanography and Paleoclimatology*, *38*(9), e2023PA004652.

Kelly, D. C., T. J. Bralower, J. C. Zachos, I. P. Silva, and E. Thomas (1996), Rapid diversification of planktonic foraminifera in the tropical Pacific (ODP Site 865) during the late Paleocene thermal maximum, *Geology*, *24*(5), 423-426.

Kelly, D. C., T. J. Bralower, and J. C. Zachos (1998), Evolutionary consequences of the latest Paleocene thermal maximum for tropical planktonic foraminifera, *Palaeogeogr., Palaeoclimatol., Palaeoecol.*, *141*, 139-161.

Kelly, D. C., T. J. Bralower, and J. C. Zachos (2001), On the demise of the early Paleogene *Morozovella velascoensis* lineage: Terminal progenesis in the planktonic foraminifera., *Palaois*, *16*, 507-523.

Kelly, D. C., T. M. J. Nielsen, H. K. McCarren, J. C. Zachos, and U. Röhl (2010), Spatiotemporal patterns of carbonate sedimentation in the South Atlantic: Implications for carbon cycling during the Paleocene–Eocene thermal maximum, *Palaeogeogr., Palaeoclimatol., Palaeoecol.*, *293*(1–2), 30-40, doi:10.1016/j.palaeo.2010.04.027.

Kennett, J. P., and L. D. Stott (1991), Abrupt deep-sea warming, palaeoceanographic changes and benthic extinctions at the end of the Paleocene, *Nature*, *353*, 225-229.

Kirtland Turner, S., P. M. Hull, L. R. Kump, and A. Ridgwell (2017), A probabilistic assessment of the rapidity of PETM onset, *Nature Communications*, *8*.

Kısakürek, B., A. Eisenhauer, F. Böhm, D. Garbe-Schönberg, and J. Erez (2008), Controls on shell Mg/Ca and Sr/Ca in cultured planktonic foraminiferan, *Globigerinoides ruber* (white), *Earth Planet. Sci. Lett.*, *273*(3–4), 260-269, doi:http://dx.doi.org/10.1016/j.epsl.2008.06.026.

Kita, N. T., T. Ushikubo, B. Fu, and J. W. Valley (2009), High precision SIMS oxygen isotope analysis and the effect of sample topography, *Chem. Geol.*, *264*(1-4), 43-57, doi:10.1016/j.chemgeo.2009.02.012.

Koch, P. L., J. C. Zachos, and P. D. Gingerich (1992), Correlation between isotope records in marine and continental carbon reservoirs near the Palaeocene/Eocene boundary, *Nature*, *358*(6384), 319-322.

Kozdon, R., T. Ushikubo, N. T. Kita, M. Spicuzza, and J. W. Valley (2009), Intratest oxygen isotope variability in the planktonic foraminifer *N. pachyderma:* Real vs. apparent vital effects by ion microprobe, *Chem. Geol.*, *258*, 327-337, doi:10.1016/j.chemgeo.2008.10.032.

Kozdon, R., D. C. Kelly, N. T. Kita, J. H. Fournelle, and J. W. Valley (2011), Planktonic foraminiferal oxygen isotope analysis by ion microprobe technique suggests warm tropical sea surface temperatures during the Early Paleogene, *Paleoceanography*, *26*(3), PA3206, doi:10.1029/2010pa002056.

Kozdon, R., D. C. Kelly, K. Kitajima, A. Strickland, J. H. Fournelle, and J. W. Valley (2013), In situ $\delta^{18}O$ and Mg/Ca analyses of diagenetic and planktic foraminiferal calcite preserved in a deep-sea record of the Paleocene-Eocene thermal maximum, *Paleoceanography*, *28*(3), 517-528, doi:10.1002/palo.20048.

Kozdon, R., D. C. Kelly, and J. W. Valley (2018), Diagenetic Attenuation of Carbon Isotope Excursion Recorded by Planktic Foraminifers During the Paleocene-Eocene Thermal Maximum, *Paleoceanography and Paleoclimatology*, *33*(4), 367-380.

Kozdon, R., D. E. Penman, D. Kelly, J. Zachos, J. H. Fournelle, and J. Valley (2020), Enhanced Poleward Flux of Atmospheric Moisture to the Weddell Sea Region (ODP Site 690) During the Paleocene-Eocene Thermal Maximum, *Paleoceanography and Paleoclimatology*, *35*(6), e2019PA003811.

Kozdon, R., and D. C. Kelly (2024a), $\delta^{13}C$ values measured by Secondary Ion Mass Spectrometry in shells of the planktic foraminifer Morozovella allisonensis from the PETM section of ODP Site 865 (Central Pacific) [Dataset]. PANGAEA, https://doi.org/10.1594/PANGAEA.967641.

Kozdon, R., and D. C. Kelly (2024b), $\delta^{13}C$ values measured by Secondary Ion Mass Spectrometry in shells of the planktic foraminifer Morozovella velascoensis from ODP Site 865 (Central Pacific) across the PETM (~56 Ma) [Dataset]. PANGAEA, https://doi.org/10.1594/PANGAEA.967640.

Kozdon, R., and D. C. Kelly (2024c), Mg/Ca ratios measured by Electron Probe Microanalyzer in shells of the planktic foraminifer Morozovella allisonensis from the PETM section of ODP Site 865 (Central Pacific) [Dataset]. PANGAEA, https://doi.org/10.1594/PANGAEA.967638.

Kozdon, R., and D. C. Kelly (2024d), Mg/Ca ratios measured by Electron Probe Microanalyzer in shells of the planktic foraminifer Morozovella velascoensis from ODP Site 865 (Central Pacific) across the PETM (~56 Ma) {Dataset]. PANGAEA, https://doi.org/10.1594/PANGAEA.967579.

Lammers, L. N., and E. H. Mitnick (2019), Magnesian calcite solid solution thermodynamics inferred from authigenic deep-sea carbonate, *Geochimica et Cosmochimica Acta*, *248*, 343-355.

Lea, D. W., T. A. Mashiotta, and H. J. Spero (1999), Controls on magnesium and strontium uptake in planktonic foraminifera determined by live culturing, *Geochimica et Cosmochimica Acta*, *63*(16), 2369-2379, doi:http://dx.doi.org/10.1016/S0016-7037(99)00197-0.

Lunt, D., H. Elderfield, R. Pancost, A. Ridgwell, G. Foster, A. Haywood, J. Kiehl, N. Sagoo, C. Shields, and E. Stone (2013), Warm climates of the past—a lesson for the future?, edited, The Royal Society.

Lunt, D. J., T. D. Jones, M. Heinemann, M. Huber, A. LeGrande, A. Winguth, C. Loptson, J. Marotzke, C. Roberts, and J. Tindall (2012), A model-data comparison for a multi-model ensemble of early Eocene atmosphere-ocean simulations: EoMIP, *Climate of the Past*.

Lunt, D. J., et al. (2016), DeepMIP: experimental design for model simulations of the EECO, PETM, and pre-PETM, *Geosci. Model Dev. Discuss.*, *2016*, 1-16, doi:10.5194/gmd-2016-127.

Lunt, D. J., M. Huber, E. Anagnostou, M. L. Baatsen, R. Caballero, R. DeConto, H. A. Dijkstra, Y. Donnadieu, D. Evans, and R. Feng (2017), The DeepMIP contribution to PMIP4: experimental design for model simulations of the EECO, PETM, and pre-PETM (version 1.0), *Geoscientific Model Development*, *10*(2), 889.

Mucci, A. (1987), Influence of temperature on the composition of magnesian calcite overgrowth precipitated from seawater, *Geochimica et Cosmochimica Acta*, *51*, 1977-1984.

Norris, R. D. (1996), Symbiosis as an evolutionary innovation in the radiation of Paleocene planktic foraminifera, *Paleobiology*, *22*, 461-480.

Oomori, T., H. Kaneshima, Y. Maezato, and Y. Kitano (1987), Distribution coefficient of Mg^{2+} ions between calcite and solution at 10-50°C, *Marine Chemistry*, *20*, 327-336.

Pagani, M., N. Pedentchouk, M. Huber, A. Sluijs, S. Schouten, H. Brinkhuis, J. S. Sinninghe Damste, G. R. Dickens, and S. Expedition (2006), Arctic hydrology during global warming at the Palaeocene/Eocene thermal maximum, *Nature*, *442*(7103), 671-675, doi:http://www.nature.com/nature/journal/v442/n7103/suppinfo/nature05043_S1.html.

Pearson, P. N., P. W. Ditchfield, J. Singano, K. G. Harcourt-Brown, C. J. Nicholas, R. K. Olsson, N. J. Shackleton, and M. Hall (2001), Warm tropical sea surface temperatures in the Late Cretaceous and Eocene epochs, *Nature*, *413*, 481-487.

Pearson, P. N., R. K. Olsson, C. Hemleben, B. T. Huber, and W. A. Berggren (2006), *Atlas of Eocene Planktonic Foraminifera*, 513 pp., Cushman Foundation Special Publication, Lawrence, Kansas.

Peng, T.-H., W. Broecker, and W. Berger (1979), Rates of benthic mixing in deep-sea sediment as determined by radioactive tracers, *Quatern. Res.*, *11*(1), 141-149.

Penman, D. E., B. Hönisch, R. E. Zeebe, E. Thomas, and J. C. Zachos (2014), Rapid and sustained surface ocean acidification during the Paleocene-Eocene Thermal Maximum, *Paleoceanography*, *29*(5), 2014PA002621, doi:10.1002/2014pa002621.

Pierrehumbert, R. T. (2002), The hydrologic cycle in deep-time climate problems, *Nature*, *419*(6903), 191-198.

Röhl, U., T. Westerhold, T. J. Bralower, and J. C. Zachos (2007), On the duration of the Paleocene-Eocene thermal maximum (PETM), *Geochem. Geophys. Geosyst.*, *8*(12), Q12002, doi:10.1029/2007gc001784.

Rush, W. D., J. T. Kiehl, C. A. Shields, and J. C. Zachos (2021), Increased frequency of extreme precipitation events in the North Atlantic during the PETM: Observations and theory, *Palaeogeogr., Palaeoclimatol., Palaeoecol.*, *568*, 110289.

Sager, W. W., E. L. Winterer, and J. V. Firth (1993), Proceedings of the Ocean Drilling Program. Initial Report 143.

Schrag, D. P., D. J. DePaolo, and F. M. Richter (1995), Reconstructing past sea surface temperatures: Correcting for diagenesis of bulk marine carbonate, *Geochimica et Cosmochimica Acta*, *59*, 2265-2278.

Sexton, P. F., P. A. Wilson, and P. N. Pearson (2006), Microstructural and geochemical perspectives on planktic foraminiferal preservation: "Glassy" versus "Frosty", *Geochemistry Geophysics Geosystems*, *7*(12), doi:10.1029/2006GC001291.

Shackleton, N. J., R. M. Corfield, and M. A. Hall (1985), Stable isotope data and the ontogeny of Paleocene planktonic foraminifera, *J. Foraminifer. Res.*, *15*(4), 321-336.

Sluijs, A., et al. (2006), Subtropical Arctic Ocean temperatures during the Palaeocene/Eocene thermal maximum, *Nature*, *441*(7093), 610-613, doi:http://www.nature.com/nature/journal/v441/n7093/suppinfo/nature04668_S1.html.

Sluijs, A., G. Bowen, H. Brinkhuis, L. Lourens, and E. Thomas (2007), The Palaeocene-Eocene Thermal Maximum super greenhouse: biotic and geochemical signatures, age models and mechanisms of, *Deep-time perspectives on climate change: marrying the signal from computer models and biological proxies*, 323.

Sluijs, A., P. K. Bijl, S. Schouten, U. Röhl, G. J. Reichart, and H. Brinkhuis (2011), Southern ocean warming, sea level and hydrological change during the Paleocene-Eocene thermal maximum, *Clim. Past*, *7*(1), 47-61, doi:10.5194/cp-7-47-2011.

Staudigel, P. T., E. H. John, B. Buse, P. N. Pearson, and C. H. Lear (2022), Apparent preservation of primary foraminiferal Mg/Ca ratios and Mg-banding in recrystallized foraminifera, *Geology*, *50*(7), 760-764.

Team, R. C. (2021), A language and environment for statistical computing, *(No Title)*.

Thomas, D. J., T. J. Bralower, and J. C. Zachos (1999), New evidence for subtropical warming during the late Paleocene thermal maximum: Stable isotopes from Deep Sea Drilling Project Site 527, Walvis Ridge, *Paleoceanography*, *14*(5), 561-570.

Thomas, D. J., J. C. Zachos, T. J. Bralower, E. Thomas, and S. Bohaty (2002), Warming the fuel for the fire: Evidence for the thermal dissociation of methane hydrate during the Paleocene-Eocene thermal maximum, *Geology*, *30*, 1067-1070.

Thomas, E. (1989), Development of Cenozoic deep-sea benthic foraminiferal faunas in Antarctic waters, in *Origins and Evolution of Antarctic Biota*, edited by J. A. Crame, pp. 283-296, Geological Society of London, Special Publication.

Tierney, J. E., J. Zhu, M. Li, A. Ridgwell, G. J. Hakim, C. J. Poulsen, R. D. Whiteford, J. W. Rae, and L. R. Kump (2022), Spatial patterns of climate change across the Paleocene–Eocene Thermal Maximum, *Proceedings of the National Academy of Sciences*, *119*(42), e2205326119.

Tripati, A. K., and H. Elderfield (2004), Abrupt hydrographic changes in the equatorial Pacific and subtropical Atlantic from foraminiferal Mg/Ca indicate greenhouse origin for the thermal maximum at the Paleocene-Eocene Boundary, *Geochemistry, Geophysics, Geosystems*, *5*(2), Q02006, doi:10.1029/2003gc000631.

Valley, J. W., and N. T. Kita (2009), *In situ* oxygen isotope geochemistry by ion microprobe, in *MAC Short Course: Secondary Ion Mass Spectrometry in the Earth Sciences*, edited by M. Fayek, pp. 16-63.

Wilson, P. A., R. D. Norris, and M. J. Cooper (2002), Testing the Cretaceous greenhouse hypothesis using glassy foraminiferal calcite from the core of the Turonian tropics on Demerara Rise, *Geology*, *30*(7), 607-610.

Zachos, J. C., M. W. Wera, S. Bohaty, M. L. Delaney, M. R. Petrizzo, A. Brill, T. J. Bralower, and I. Premoli-Silva (2003), A transient rise in tropical sea surface temperature during the Paleocene-Eocene Thermal Maximum, *Science*, *302*, 1551-1554, doi:10.1126/science.1090110.

Zachos, J. C., et al. (2005), Rapid Acidification of the Ocean During the Paleocene-Eocene Thermal Maximum, *Science*, *308*(5728), 1611-1615, doi:10.1126/science.1109004.

Zachos, J. C., S. Schouten, S. Bohaty, T. Quattlebaum, A. Sluijs, H. Brinkhuis, S. J. Gibbs, and T. J. Bralower (2006), Extreme warming of mid-latitude coastal ocean during the Paleocene-Eocene Thermal Maximum: Inferences from TEX_{86} and isotope data, *Geology*, *34*(9), 737-740, doi:10.1130/G22522.1.

Zachos, J. C., S. M. Bohaty, C. M. John, H. McCarren, D. C. Kelly, and T. Nielsen (2007), The Palaeocene–Eocene carbon isotope excursion: constraints from individual shell planktonic foraminifer records, *Philosophical Transactions of the Royal Society A: Mathematical, Physical and Engineering Sciences*, *365*(1856), 1829-1842, doi:10.1098/rsta.2007.2045.

Zeebe, R., A. Ridgwell, and J. Zachos (2016), Anthropogenic carbon release rate unprecedented during the past 66 million years, Nat. Geosci., 9, 325–329, edited.

Zeebe, R. E., J. C. Zachos, and G. R. Dickens (2009), Carbon dioxide forcing alone insufficient to explain Palaeocene-Eocene Thermal Maximum warming, *Nature Geoscience*, *2*, 576-580, doi:10.1038/NGEO578.

Zeebe, R. E., and L. J. Lourens (2019), Solar System chaos and the Paleocene–Eocene boundary age constrained by geology and astronomy, *Science*, *365*(6456), 926-929, doi:10.1126/science.aax0612.

Zhang, Q., L. Ding, K. Kitajima, J. W. Valley, B. Zhang, X. Xu, H. Willems, and A. Klügel (2020), Constraining the magnitude of the carbon isotope excursion during the Paleocene-Eocene thermal maximum using larger benthic foraminifera, *Global Planet. Change*, *184*, 103049.